Arch. Mech., 50, 1, pp. 21–40, Warszawa 1998
FIFTY YEARS OF THE ARCHIVES OF MECHANICS

Continuum damage and failure evolution in inhomogeneous ceramic rods

J. NAJAR and V. SILBERSCHMIDT (MUNICH)

A WELL-POSED CDM model and an adequate representation of deterministic and random inhomogeneity factors, combined with an efficient numerical algorithm of modified lattices, yield a realistic simulation of the rupture properties of alumina ceramic specimens at tensile tests. Effects of energy dissipation and acoustic emission, the load-carrying capacity and the post-critical response are analysed in dependence of the heterogeneity realisations, which are related to the initial damage distribution within the specimen. This distribution is shown to be a crucial factor determining the response of brittle damaging ceramics at rupture.

1. Introduction

THE MECHANICAL RESPONSE and failure of brittle materials, monolithic alumina ceramics in particular, are commonly described by means of linear elasticity capped by some rupture condition [1]. Basically, models of this kind are not in the position to explain various experimental observations; these are e.g. acoustic emission and energy dissipation at subcritical loads [2, 3], excessive energy spent at rupture, as compared with single crack-based fracture energy estimates [4], post-critical response [5], size effects in the rupture strength [6], and many others. On the other hand, continuum damage mechanics (CDM) models [7], although reflecting some of the above effects, seem to be not flexible enough to encompass the whole variety of experimental observations, as long as the most fundamental feature of these materials, namely, their inhomogeneity, is not properly accounted for.

The aim of the present paper is to show that a well-posed continuum damage model, [8, 9], and an adequate representation of the deterministic and stochastic factors influencing the inhomogeneity of a sintered ceramic rod, combined with an efficient numerical procedure, result in a realistic simulation of the rupture properties of an alumina specimen in uniaxial tension. The results show also the influence of various realisations of the inhomogeneity on the rod rupture evolution.

The calculations presented in the paper are based on the simulations of the experimental results, [4], obtained with sintered cylindrical specimens of alumina ceramics (diameters 4 to 12 mm, grain size $10 - 20\,\mu$m, tensile strength ca. 300 MPa, compressive strength ca. 3000 MPa, Young modulus 350 GPa); for computational details see [10]. Micromechanical aspects of the damage model

[8, 9], to be presented in Sec. 2, are not discussed in the paper. The applied discretisation, Sec. 3.1, represents rather a mesoscale model (discrete element size ca. 300 μm as compared to the grain size), mainly of the inhomogeneity and randomness of mechanical parameters, Sec. 3.2, as well as mechanisms of local failure development and energy balance of interactions between the elements, Sec. 3.4.

2. Damage evolution law and local failure condition

Basic results on the continuum damage model for brittle ceramics presented in [8, 9] are recalled and extended in this section. The stress-strain relation for uniaxial tensile loading

$$\sigma = E(1 - D)\varepsilon, \tag{2.1}$$

contains the damage variable D, which is governed by the damage evolution law

$$D = D_0 \exp\left(\frac{E\varepsilon^2}{2W^*}\right). \tag{2.2}$$

Here, D_0 denotes the initial damage at the onset of the tensile deformation ε in the current tensile loading branch of the process; the parameter W^*, characterising material's intake of the energy at damage, is denoted further as damage absorbing capacity. The stress-strain relation at damage (2.1) – (2.2) reaches a maximum, see Fig. 1, at the damage value D_m, which can be calculated from the relation

$$D_m \exp\left(\frac{D_m - 1}{2D_m}\right) = D_0\,, \tag{2.3}$$

depending thus solely on the initial damage D_0. The corresponding values of stress σ_m and strain ε_m characterise the load-carrying capacity and material's compliance. The latter can be expressed as a function of initial damage D_0 by the relation

$$\varepsilon_m = \sqrt{\frac{2W^*}{E}}\sqrt{\ln\frac{D_m}{D_0}}\,. \tag{2.4}$$

Expressions (2.3), (2.4) serve as the basis for the determination of the failure criterion in damage. It can be shown, namely, that shortly beyond the stress maximum (m) the uniaxial extension becomes unstable at a point (s) of a strain-controlled process, Fig. 1. Therefore, it can be further assumed that at arriving at the (m)-point, the material undergoes a rapid decay and the damage grows from the value D_m to the nominal value $D = 1$ corresponding to complete

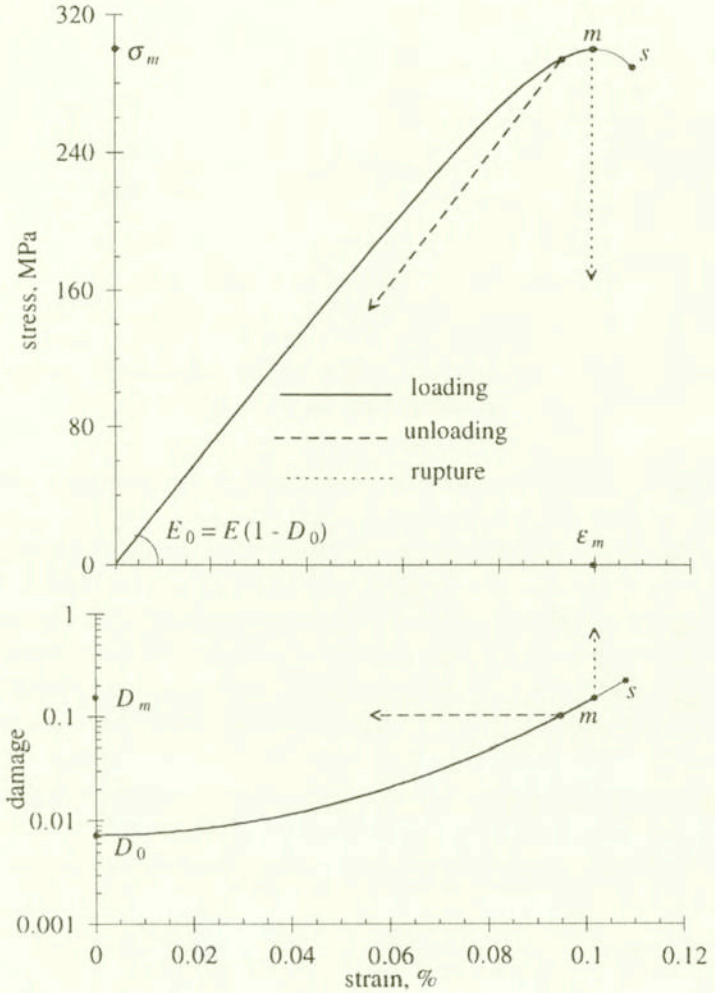

FIG. 1. Stress- and damage-strain curves at tensile loading, unloading and rupture; data for alumina ceramics: $E = 350\,\mathrm{GPa}$, $W^* = 59\,\mathrm{kJ/m^3}$; initial damage $D_0 = 0.73\%$ corresponds to $\sigma_m = 350\,\mathrm{MPa}$ and $\varepsilon_m = 0.1\%$.

failure. Although at increasing initial damage D_0 the failure damage D_m also increases, cf. Eq. (2.3), the load-carrying capacity σ_m and the strain at failure ε_m drop substantially, Fig. 2.

At a strain increment from ε_1 to ε_2, deformation work is performed

$$\Delta W_\sigma = \int_{\varepsilon_1}^{\varepsilon_2} \sigma \, d\varepsilon = \frac{E}{2}\left(\varepsilon_2^2 - \varepsilon_1^2\right) - D_0 W^* \left(\exp\frac{E\varepsilon_2^2}{2W^*} - \exp\frac{E\varepsilon_1^2}{2W^*}\right). \tag{2.5}$$

It can be split into increments of recoverable strain energy ΔW_r and the dissipation related to material damage and associated acoustic and heat losses [8].

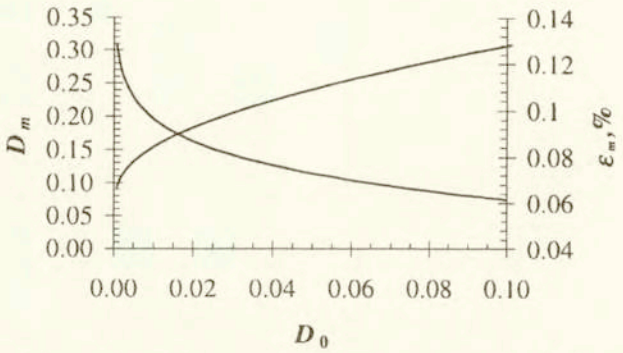

FIG. 2. Damage D_m and strain ε_m at failure, in dependence of the initial damage D_0 (data for alumina, see Fig. 1).

At modest compressive loads, or in unloading from tensile branches of the process, the ceramics follow the incremental Hooke's law $\Delta\sigma = E\Delta\varepsilon$, where E denotes the Young's modulus of the undamaged material [8]; here, no change of damage and no dissipation increment take place. The recoverable strain energy released at complete unloading from a stress σ equals $\sigma^2/2E$. Failure at σ_m leads to the release of the whole stored energy $\sigma_m^2/2E$ in a violent event.

Consider partial unloading from the state characterised by stress σ and damage D to the stress $\sigma_* > 0$, see Fig. 3. Under the branch-invariance conditions discussed in [9], it follows that the state of damage remains unchanged, i.e. $D_* = D$; the strain ε_* undergoes a shift $\delta\varepsilon_s$ to a secondary state of reference 0_s, from which the secondary strain ε_s is counted. The secondary state corresponds also to a secondary initial damage value D_{0s}. The following relations are valid for these quantities:

$$\varepsilon_* = \frac{\sigma_*}{E} + \varepsilon D, \tag{2.6}$$

$$\varepsilon_s = \frac{\varepsilon_* - \varepsilon D}{1 - D}, \tag{2.7}$$

$$\Delta\varepsilon_s = \frac{D}{1 - D}(\varepsilon - \varepsilon_*), \tag{2.8}$$

$$D_{0s} = D \exp\left(-\frac{E\varepsilon_s^2}{2W^*}\right). \tag{2.9}$$

During the partial unloading, the following amount of strain energy is released, see Fig. 3:

$$\Delta W_r = \frac{1}{2E}\left(\sigma^2 - \sigma_*^2\right) = \frac{E}{2}\left[\varepsilon_* + \varepsilon(1 - 2D)\right](\varepsilon - \varepsilon_*). \tag{2.10}$$

The tensile reloading branch, which begins at the state (σ_*, D) is governed by the branch-invariant relations Eq. (2.1) – (2.4), as applied to the secondary initial

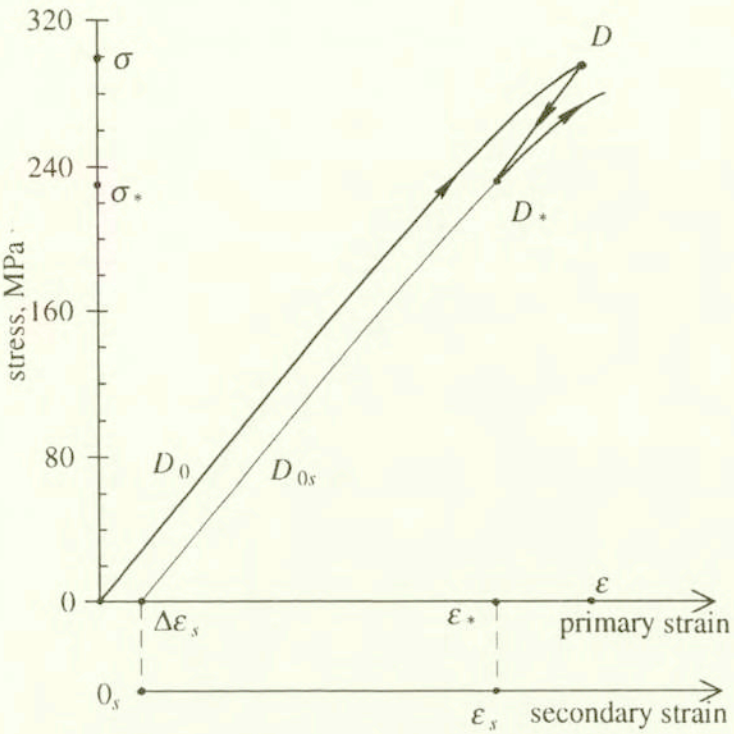

FIG. 3. Partial unloading and reloading in tension (data for alumina, see Fig. 1); the secondary reference state 0_s corresponds to the strain shift $\Delta\varepsilon_s$, Eq. (2.8).

damage D_{0s} and the secondary strain ε_s, while preserving the material parameters E and W^*.

3. Formulation of the problem

A ceramic cylindrical rod will be considered under the conditions of a uniform extension. The modelling of the rod inhomogeneity within its cross-section is based on the combination of a discretization procedure, given in Sec. 3.1, and the material modelling presented in Sec. 2, as applied to single discrete elements. This is complemented by an analysis of the initial damage distribution within a ceramic rod based on experimental data, Sec. 3.2, and by modelling of element's interactions at extension and local failures, Sec. 3.4.

3.1. Discretization

A nonuniform distribution of microdefects in a ceramic rod must result in its inhomogeneous response even at uniform uniaxial extension. A $2d$-formulation, with parameters of the ceramics depending on the position within the cross-section, becomes thus necessary for the analysis of its damage evolution. Such

formulation is implemented in this paper for a cylindrical rod by means of a cross-section discretization into elements of equal area, Fig. 4. The size of the elements must secure the applicability of the continuum damage model presented in Sec. 2. In the following computations, corresponding to the evaluations of the ceramics test presented in [4], the typical size of the elements is ca. 300 μm, as compared to the grain size of the alumina not exceeding 20 μm, which seems to fit well the above mentioned condition. A $3d$-discretization, although basically possible, is not presently considered due to the lack of particular data on the axial distribution of the inhomogeneities along ceramic specimens under investigation.

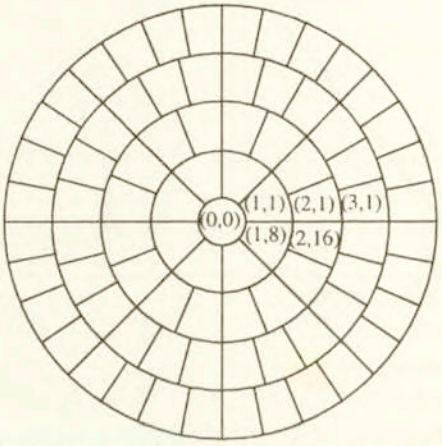

FIG. 4. Cross-section discretisation for $N = 4$, $M = 81$; double indexation of elements facilitates the local failure interaction analysis, see Sec. 3.4.

The cross-section of radius R is divided into N rings of elements, with a circular central element of radius $r_0 = R/(2N + 1)$; all other elements have the radial height $h = 2r_0$ and the angular width $\theta_k = \pi/4k$. Here, k denotes the ring number, with $k = 1$ for the ring next to the central element and $k = N$ for the external ring. The cross-section is divided thus into $M = 1 + 8\sum_{k=1}^{N} k$ elements, each having the same area of $\pi R^2/M$. Element dimensions are chosen to meet the requirements for a representative unit cell, being small enough with respect to the characteristic length R of the macroscopic field of the rod, and sufficiently large as compared to the size of the microscopic structure of the ceramic material.

3.2. Inhomogeneity

Two main factors determine the features of the distribution of mechanical properties in the rod cross-section:

a) general heterogeneity, linked to the randomness of imperfections in ceramics [11];

b) specific radial distribution, due to the rod-manufacturing technology.

For the case under study, we may assume that all the nonuniformity of the process is based on the features of the initial damage distribution. For the given ceramic material it is, namely, this parameter that influences both the damage accumulation and the response at failure, see Sec. 2. Introducing a $2d$-distribution of initial damage, and putting it at the basis of the two above factors, we express the rod response problem in terms of a $2d$ stochastics.

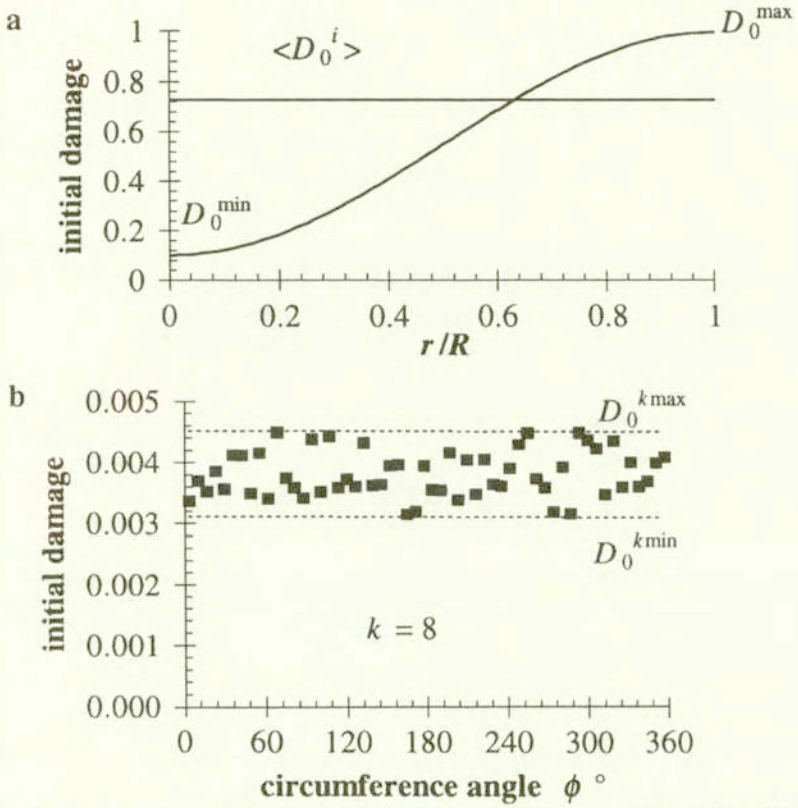

FIG. 5. Initial damage distributions: a) deterministic, over rod radius; b) random, over circumference; exemplary realisation at ring $k = 8$, with scatter band width constant $k_s = 0.1$.

In order to model the D_0-distribution, we recall the elementary notion of damage as a volumetric ratio of voids in a material [12]; the ratio is inversely related to the material's density. We take the radial distribution of density in sintered rods [13] with its drop from the centre to the periphery of the specimen as indicative for the following initial damage function of the radius r:

$$D_0(r) = D_0^{\min} + (D_0^{\max} - D_0^{\min}) \sin^2 \frac{\pi r}{2R}. \tag{3.1}$$

Here, $D_0^{\min}$ relates to the maximum material density, i.e. to the lowest level of initial defects, in the rod centre, while $D_0^{\max}$ corresponds to lower density at

$r = R$, Fig. 5 a. A reference value

$$\overline{D}_0 = \frac{1}{A}\int_A D_0\, dA = \langle D_0^i \rangle\Big|_{M\to\infty} \tag{3.2}$$

for the distribution (3.1) is given by

$$\overline{D}_0 = D_0^{\min} + \left(D_0^{\max} - D_0^{\min}\right)\left(\frac{2}{\pi^2} + \frac{1}{2}\right),$$

corresponding in the discretization to the $M \to \infty$ limit of the initial damage D_0^i $(i = 1, ..., M)$ averaged over all M elements; (3.2) means averaging over the cross-section area A. The reference quantity $\overline{D}_0$ can be used for comparing various discretization and statistical realisations.

To account for the randomness in the $2d$-distribution of defects, we introduce a stochastic sample of the initial damage within each ring separately. It is based on the experimental observations, [13, 14], showing a substantial density scatter within sintered specimens. Here, uniform probability distribution of D_0 within a range $[D_0^{k\,\min}; D_0^{k\,\max}]$ is assumed for each k-th ring separately. The bounds are related to the $D_0(r)$-dependence given by Eq. (3.1), and take the form

$$\left.\begin{matrix} D_0^{k\,\min} \\ D_0^{k\,\max} \end{matrix}\right\} = D_0(r_0(2k \mp 1))(1 \mp k_s), \tag{3.3}$$

where k_s is a scatter band width constant. In numerical simulations, a random number generator is used for the distribution of initial damage. A typical distribution is shown in Fig. 5 b.

3.3. Damage evolution in elements

The cross-section discretization and the distribution of D_0^i over the elements imply the application of the constitutive equations (2.1) – (2.3) to each i-th element separately in the form

$$\begin{aligned} \sigma^i &= E(1 - D^i)\varepsilon, \\ D^i &= D_0^i \exp\left(\frac{E\varepsilon^2}{2W^*}\right), \\ D_m^i \exp\left(\frac{D_m^i - 1}{2D_m^i}\right) &= D_0^i, \qquad i = 1, ..., M_0\,. \end{aligned} \tag{3.4}$$

It is assumed here that all the elements in the cross-section are exposed to the same external strain ε. They exhibit the same material properties regarding the elasticity modulus E and the damage absorbing capacity W^*. The differences in the response of the elements are in the first stage of the loading solely due to the initial damage distributions (3.2) – (3.3).

The situation changes somewhat as soon as the rod extension ε arrives at the strain-at-failure ε_m^w of the weakest w-th element with the highest initial damage within the cross-section, cf. Eq. (2.4). In order to further the numerical simulation of the rod response under tension, Eqs. (3.4) need to be now completed by interaction-at-failure conditions for the elements.

3.4. Local failure and interaction of elements

Until the failure of the w-th element, see Sec. 3.3, there is no interaction between the uniformly extended finite elements assumed to be in the uniaxial state of strain. With the failure of the first element, considered within the framework of the damage model described in Sec. 2, the standard situation is the following one: an i-th element, with a higher initial damage D_0^i than all p elements in its vicinity, reaches its respective failure strain ε_m^i sooner than any j-th element of the neighbourhood, compare Eq. (2.4) and Fig. 2. Upon reaching the state of failure, the element loses its carrying capacity, and its damage catastrophically grows from D_m^i to the nominal level $D^i = 1$ corresponding to $\sigma^i = 0$, see Eq. (2.1).

Such events occur randomly in various regions of the cross-section and at various instants of the strain history. Each spatially separate event increases the connectivity of the region under study. These features make the use of established numerical codes based on the finite elements method (FEM) rather cumbersome; the modelling would demand a reformulation of the boundary-value problem nearly at each strain step after the first element's failure. An alternative is provided by utilisation of the modified lattice algorithms, developed originally in statistical physics, and lately applied in stochastic fracture problems, [15, 16]. An advantage of this approach lies in the possibility to analyse highly heterogeneous media and complicated failure morphology. Recently, this modelling approach has been considered in the analysis of the macroscopic response to the development of defect ensembles in disordered brittle materials under stress-controlled tension [17, 18], as a unification of the CDM and lattice algorithms.

In order to describe the strain-controlled process, the following simplified algorithm is suggested, Fig. 6. The failure of the i-th element results in a violent release of its stored elastic energy, ${\sigma_m^i}^2/(2E)$, see Sec. 2. The energy is transferred to p nearest neighbours possessing a common boundary with the failed one. It is equally partitioned between them, independently of the size of their contact. The j-th element, which has been in the state *1*, $(\varepsilon, \sigma_1^j, D_1^j)$, receives thus at best a $(1/p)$-th share of the released energy. Under unconstrained circumstances, the energy share is transformed into the deformation work performed on the j-th element, see the area under the stress-strain curve segment *1* – *2*, Fig. 6. The state *2*, $(\varepsilon_2^j, \sigma_2^j, D_2^j)$, corresponds to the increments in strain $\delta\varepsilon^j$, stress $\delta\sigma^j$ and damage δD^j, cf. Eqs. (2.5) and (3.4).

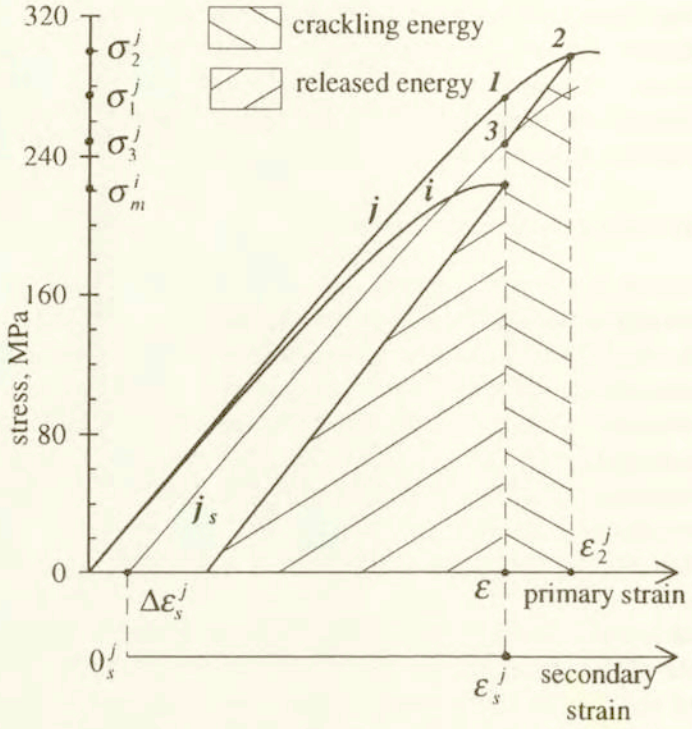

FIG. 6. Energy release at failure of the i-th element and interaction with the j-th element: loading *1* – *2*, unloading *2* – *3*, acoustic crackling emission.

Due to the kinematical constraint of the common external strain ε, however, the j-th element must undergo simultaneously an unloading by the strain decrement $-\delta\varepsilon^j$, resulting in the relaxation path *2* – *3*, Fig. 6. The element returns to the strain ε, although at lower stress σ_3^j, and remains at the damage value of $D_3^j = D_2^j$. The energy released at this relaxation process, cf. Eq. (2.10), causes acoustic effects, further referred to as crackling.

The energy flux due to the failure of one element induces thus in all neighbouring elements transitions analogous to the path *1* – *2* – *3*: from their respective states *1*, the elements undergo intermediate loading *1* – *2*, followed by relaxation *2* – *3*. Has one of the neighbouring elements been already broken in a previous event, its share of the violently released energy is irradiated directly into the environment as an acoustic snap.

The energy balance for the j-th element in the vicinity of the failed i-th element is

$$\frac{E}{2}\left(\varepsilon_2^{j\,2} - \varepsilon^2\right) - D_0^j W^* \left(\exp\frac{E\varepsilon_2^{j\,2}}{2W^*} - \exp\frac{E\varepsilon^2}{2W^*}\right) = \frac{\sigma_m^{i\,2}}{2Ep} \tag{3.5}$$

cf. (2.5), and yields the strain ε_2^j at the state *2*. The resulting damage in state *3*

$$D_3^j = D_2^j = D_0^j \exp\left[\frac{E{\varepsilon_2^j}^2}{2W^*}\right] \tag{3.6}$$

and the relaxation *2* - *3* lead to a secondary state of reference [9], with a strain shift

$$\Delta\varepsilon_s^j = \frac{D_2^j}{1 - D_2^j}\left(\varepsilon_2^j - \varepsilon\right), \tag{3.7}$$

cf. Eq. (2.8) and Fig. 3, and to a secondary initial damage, cf. Eq. (2.9)

$$D_{0s}^j = D_3^j \exp\left[-\frac{E{\varepsilon_s^j}^2}{2W^*}\right], \tag{3.8}$$

where $\varepsilon_s^j = \varepsilon - \Delta\varepsilon_s^j$ is the secondary strain in the j-th element, cf. Sec. 2.

The damage increment in the j-th element may lead to the damage D_3^j, Eq. (3.6), exceeding the respective damage at failure $D_m^j(D_{0s}^j)$, see Eqs. (3.4) and (3.8). This would mean that the local failure of the i-th element induces the failure of the j-th element. The latter, in its turn, may further induce failures in its own neighbourhood. Thus, a cascade of events of local failures can be generated.

4. Numerical realisation and results

In the numerical realisation, extension of a cylindrical rod made of alumina ceramics Al23 (Frialit - Degussit), tested in [4], has been modelled. The material data E and W^* have been taken according to the average response of the tested specimens. At 12 mm diameter, the cross-section has been divided into 20 rings with 1521 elements, cf. the procedure of Sec. 3.1. The characteristic size of the element is thus about 300 μm, i.e. by an order of magnitude larger than the mean grain size (10 – 20 μm) in the ceramics, allowing for the application of the CDM model to single elements. A program assigns to each element not only its "global" number from 1 to M but also a pair of indices, cf. Fig. 4, denoting its ring and position within the ring. An effective algorithm for finding the nearest neighbours has been based on it, generalising the experience with orthogonal grids in [17, 18].

In the first step, initial values of damage D_0^j are distributed with the use of a random number generator on the basis of relations (3.1), (3.3). In the following examples, we take $k_s = 1$, which results in the presence of some initially undamaged elements in each ring and thus in an overestimation of the post-critical

deformation. In order to exclude the effect of the variation of the mean value

$$\langle D_0^i \rangle = \frac{1}{M} \sum_{i=1}^{M} D_0^i \tag{4.1}$$

for different realisations, the random values D_0^i are corrected by multiplication with a renormalisation parameter $k_{\text{ren}} = \overline{D}_0 / \langle D_0^i \rangle$, cf. Eq. (3.2).

The next step is the determination of the local failure conditions for all elements from the relation $(3.4)_3$. Applying in steps equal strain increments $\Delta\varepsilon$ to all elements, we obtain that damage evolves with different rates, see Eq. $(3.4)_2$, due to different initial conditions. The evolution in the elements is independent of each other up to the moment of the first local failure.

Here, a transition according to Sec. 3.4 takes place in the neighbourhood of the weakest element $w = i$. The solution of Eq. (3.5) with respect to ε_2^j is carried out by an iterative Newton procedure, until the criterion $\|\varepsilon_2^{j(q+1)} - \varepsilon_2^{j(q)}\| \leq \alpha\varepsilon$ is fulfilled. Here, q is the step of iteration, parameter α equals 10^{-6} in our simulations.

After each event of local failure and interaction, see Sec. 3.4, the neighbourhood is examined with the purpose to check the induced failure conditions, and to account for the possibility of a failure cascade. After the completion of all cascades within the current step, the value of the load is computed as

$$F = A_{\text{el}} \sum_{i=1}^{M} \sigma^i,$$

where A_{el} is the element area. Also, the current damage level D is obtained by averaging of D^j over all elements by a formula analogous to Eq. (4.1), and the number of failed elements n is calculated in the cross-section. To the elements, which have undergone the *1 - 2 - 3* - transition, the algorithm assigns their secondary strain ε_s and secondary initial damage D_{0s} values to be reckoned with at further steps.

At this instance, the algorithm goes into the next step, resulting in dependences $F(\varepsilon)$, $D(\varepsilon)$ and $n(\varepsilon)$, see Fig. 7. The load-strain relation, Fig. 7 a, demonstrates a response that is characteristic for brittle ceramics [1]: a practically linearly ascending loading curve arrives at the limit which may be identified with rupture load, followed by a rapid descent. The latter can be roughly subdivided into two stages: a sharp drop after the rupture load, and a tail of dropping residual load-carrying capacity. This result follows alone from the collective response of the set of elements exhibiting the CDM properties under consideration: no specific rod rupture cap was needed in these simulations.

A comparison of $F(\varepsilon)$ with $D(\varepsilon)$ and $n(\varepsilon)$ explains the strongly non-linear behaviour. After the monotonous damage accumulation, stage 1, Fig. 7 b-c, a substantial share of elements approaches the pre-failure state. A relatively small

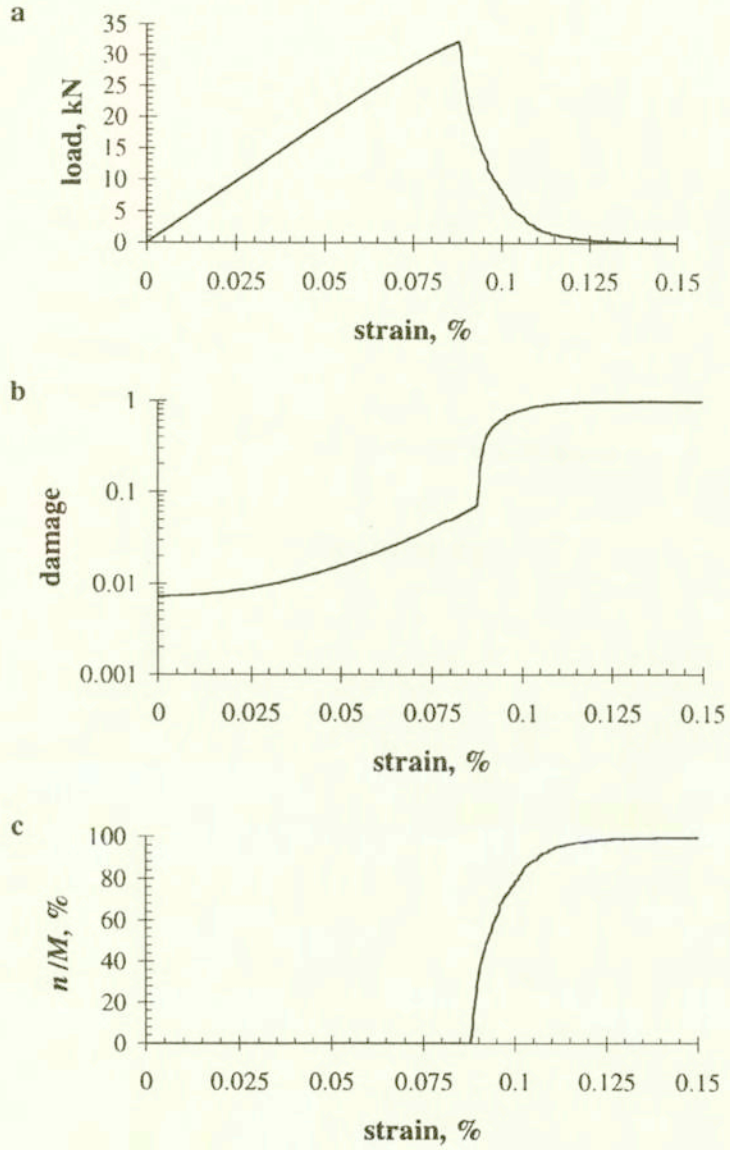

FIG. 7. Computational results for $\overline{D}_0 = 0.73\%$, in a 12 mm diameter ceramic rod (data for alumina, see Fig. 1): a) load F, b) mean damage D, c) number of failed elements n, as function of rod extension ε.

increase in the strain ε causes now an extensive process of element failures, stage 2, enhanced by the energy release effects, Sec. 3.4. Elements with low initial damage (close to $\inf_k D_0^{k\,\min}$) are responsible for the third characteristic stage of the curve: an extended post-critical response of the few remaining elements. These three stages are reflected also in the $D(\varepsilon)$ diagram, see Fig. 7 b.

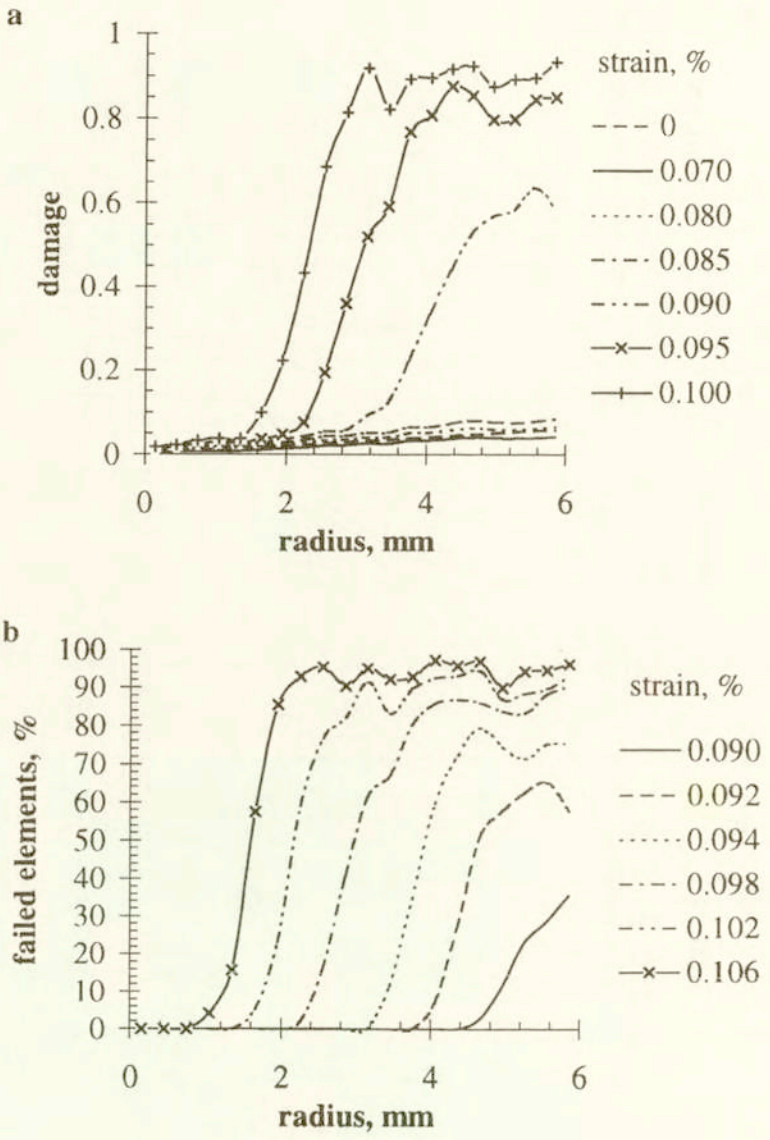

FIG. 8. Radial distributions of (a) the damage (mean values in rings) and (b) the number of failed elements (percentage of elements in rings), in dependence of rod extension.

Figure 8 demonstrates the evolution of radial distributions of damage and of the number of failed elements in rings. It is obvious, that damage at the stage 2 of extensive failure shows a high extent of localisation in peripheral rings (here: above $\varepsilon = 0.085$, Fig. 8 a). This is also reflected in the localisation of the number of failed elements (Fig. 8 b): failures occur initially in external rings only; with the strain development they increasingly take place in the central rings.

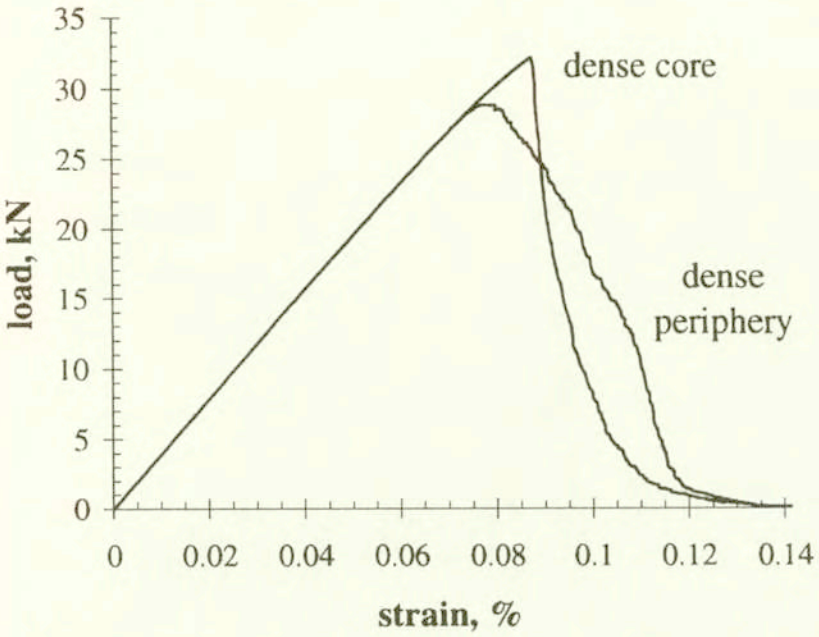

FIG. 9. Comparison of load-extension curves (specimen data, see Fig. 7) for two opposite radial distributions of the initial damage D_0 at the same value $\overline{D}_0 = 0.73\%$; for the dense core specimen, see Eq. (3.1); for the dense periphery specimen, $D_0^{\max}$ is at $r = 0$.

In order to analyse the effect of the type of randomness on the mechanical response of ceramics, let us study an opposite radial distribution of initial damage. We assume now the maximum of D_0 in the rod centre, and its minimum in external rings, i.e. consider a rod with a denser periphery than its core, compare Sec. 3.2. The resulting rupture load and the post-critical response, Fig. 9, differ substantially from the previously studied case. At the same level of mean initial damage $\overline{D}_0$, Eq. (3.2), the load-carrying capacity of the rod with a more porous core is by 10.3 percent lower than that for a more dense core, and the respective strain value is also lower by 9.5 percent. On the other hand, the descending branch of the $F(\varepsilon)$-curve is more protracted for the rod with more porous core.

The analysis of the released acoustic energy at failure evolution, Fig. 10, obtained by our numerical simulation, reflects the non-uniformity of the process. The distribution of the irradiated energy density over the strain closely reminds the data on acoustic emission in ceramics [2, 3]. With the progress of rod extension, the snapping component of the energy increases faster than the crackling one, cf. Sec. 3.4. It is the result of the advancing failure of elements and the increase of the connectivity of the cross-section, at which the relative portion of unbroken elements in immediate neighbourhoods at local failure events continuously diminishes.

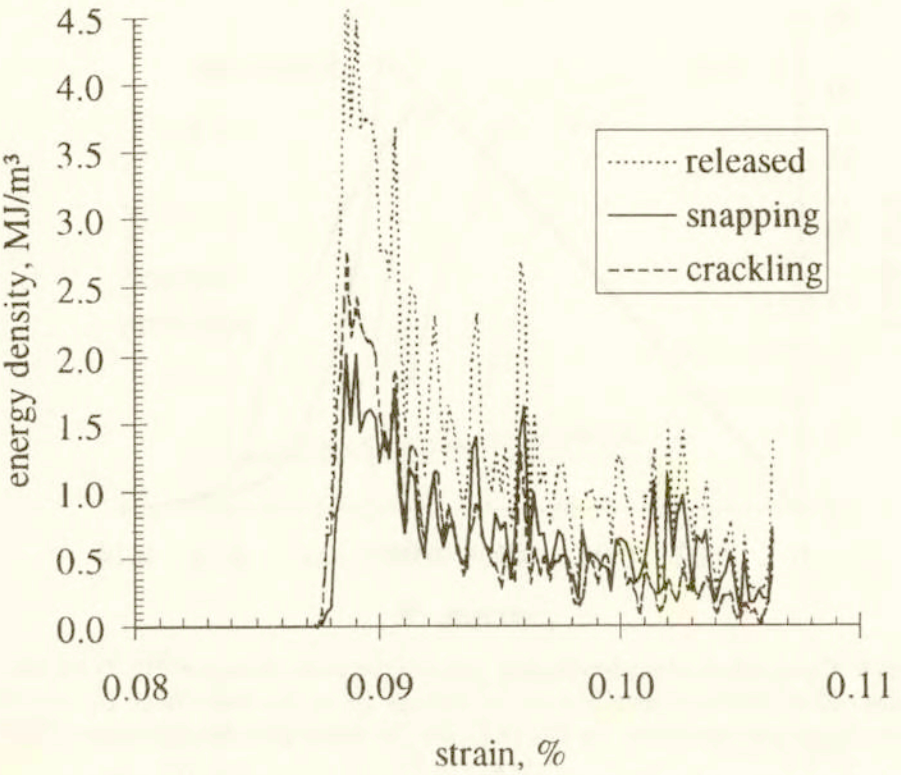

FIG. 10. Energy release at elements' failure, interpreted as acoustic effects of crackling and snapping, as functions of rod extension.

One of the much discussed problems of the mechanical response of damaging materials is the analysis of their unloading properties in the post-critical state. According to most CDM models, e.g. [7], the unloading modulus of a damaged material is $E_u = E(1 - D_u)$, where D_u denotes the damage at unloading. The non-unique relation between E_u and D_u would yield thus the basis for experimental determination of damage, mostly for ductile materials, [7]. Experimental data on unloading in brittle materials are limited mainly to the bending of notched specimens with initial cracks [5], while data on uniaxial tensile tests with smooth specimens are practically nonexistent due to the difficulties, [19], connected with the extremely low strain-to-failure values in ceramics and to their rapid rupture.

In our numerical simulations, unloading was performed at a certain share of failed elements (between 5 and 70 percent) in the cross-section, Fig. 11. Thus, the unloading begins at some load F_u and strain ε_u of the descending branch of the load characteristic, and can be characterised by the corresponding mean damage D_u exceeding the damage at the onset of rupture. The slopes of the unloading branches steadily decrease with the increase of D_u and with the advance of the rupture. They yield some non-vanishing residual strain ε_r, which seems to

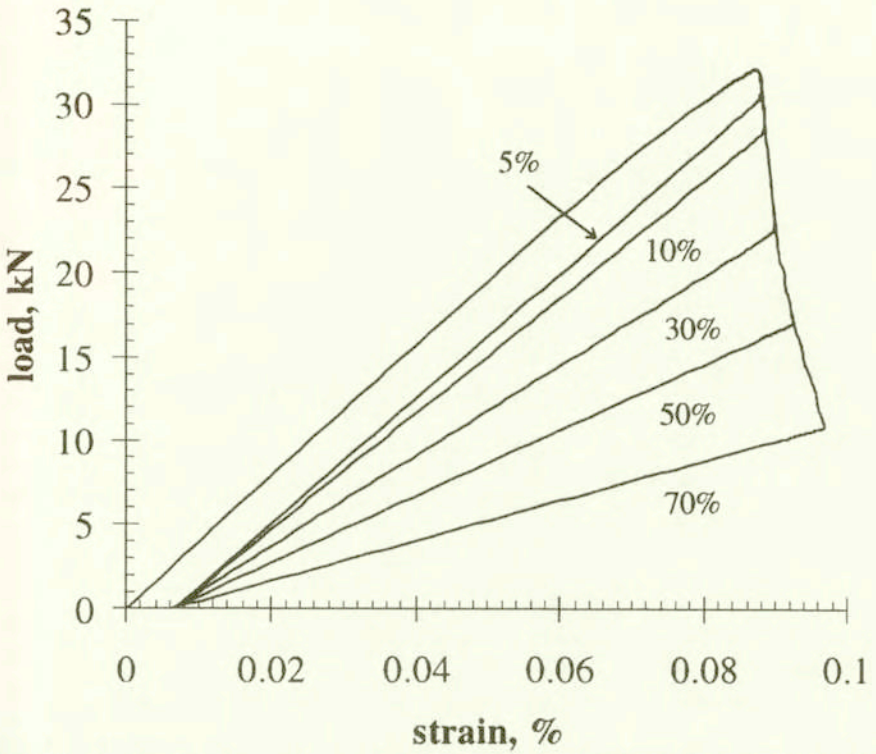

FIG. 11. Unloading characteristics at a given percentage number of failed elements (specimen data, see Fig. 7).

be nearly independent of D_u, although it clearly depends on the choice of the inhomogeneity realisation, cf. Fig. 9.

However, the dependence of the unloading slope on the mean damage at unloading D_u differs substantially from the predictions in [7]. Moreover, there is an obvious difference in the dependence of the slope on D_u for the two different inhomogeneity realisations discussed above. Let us compare the mean unloading modulus

$$E_u = \frac{F_u}{A(\varepsilon_u - \varepsilon_r)}$$

with the value $E(1 - D_u)$, as predicted in [7]; Fig. 12 presents their ratio against the mean damage at unloading D_u. We observe that in both inhomogeneity realisations, the unloading modulus steadily exceeds the predictions by values up to more than 10 per cent. This indicates that a phenomenological extraction of the damage values from measurements in unloading must be done with care; it may yield doubtful results when no data on the inhomogeneity distribution in specimens are available.

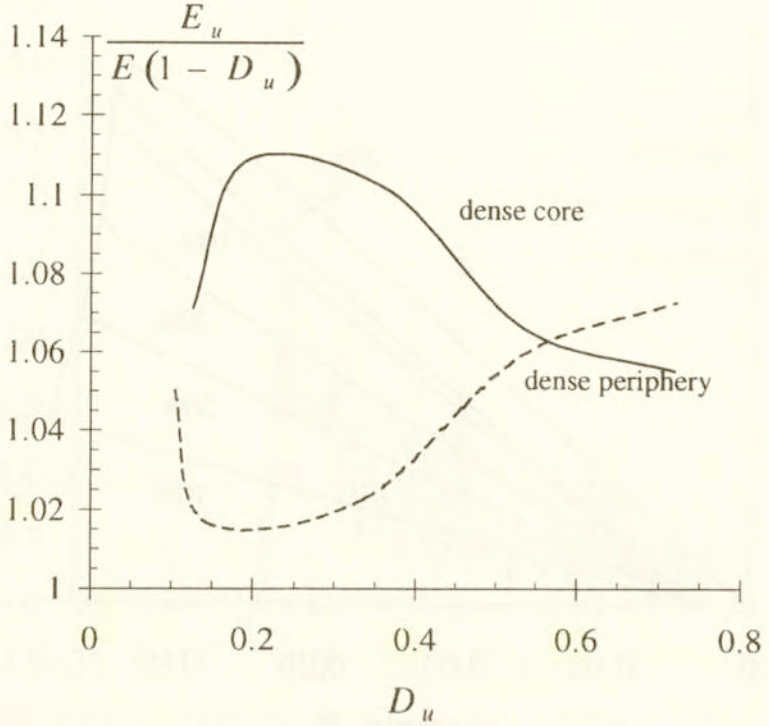

FIG. 12. Comparison of the mean unloading modulus E_u and the quantity $E(1 - D_u)$ based on the mean damage D_u at unloading, for two radial distributions of D_0, compare Fig. 9.

5. Conclusions

The proposed 2*d* approach, based on the damage evolution law [8] as applied to a set of discrete elements with deterministically and randomly distributed initial damage, allows for efficient numerical simulations of a whole range of characteristic response features of brittle specimens. The qualitative differences in response between homogeneous and heterogeneous specimens become quite obvious in the proposed numerical procedure, [17], since the process can be followed in all details concerning each single element of the system.

For the particular problem under consideration, it has been shown that certain characteristics of the damage evolution and rupture strongly depend on the kind of the cross-section heterogeneity of the specimen. This should be treated as a call for caution at certain CDM interpretations of experimental results, which may lead to doubtful conclusions when the type of inhomogeneity within the tested specimens is not known *a priori*.

The tensile rod simulations presented here can easily be extended to the study of heterogeneity scale effects, i.e. the dependence of the rupture strength on the

specimen size, [10], damage evolution and failure in ceramic beams and similar problems. The procedure contains further capabilities with regard to unloading and reloading under strain-controlled conditions, being thus potentially applicable to problems of cyclic fatigue. Finally, the applications of the procedure in composite mechanics represent an obviously important field of further research.

References

1. M.V. SWAIN [Ed.], *Structure and properties of ceramics*, Material Science and Technology, Vol. 11, VCH, Weinheim 1994.
2. L.J. GRAHAM and G.A. ALERS, *Microstructural aspects of acoustic emission generation in ceramics*, [in:] Fracture Mechanics of Ceramics. Volume 1. Concepts, Flaws and Fractography, R.C. BRANDT, D.P.H. HASSELMAN and F.F. LANGE [Eds.], pp. 175–188, Plenum Press, New York - London 1973.
3. M.J. NOON and R.R. MEHAN, *Observation of crack propagation in polycrystalline ceramics and its relationships to acoustic emissions*, [in:] Fracture Mechanics of Ceramics. Volume 1. Concepts, Flaws and Fractography, R.C. BRANDT, D.P.H. HASSELMAN and F.F. LANGE [Eds.], pp. 201–229, Plenum Press, New York - London 1973.
4. S. BIERWIRTH, *Verfahren zur Bestimmung dynamischer Zugbruchparameter von Hochleistungskeramik*, VDI Verlag, Düsseldorf, **18**, 148, 1994.
5. R.W. STEINBRECH, A. REICHL und W. SCHAARWÄCHTER, *Einfluß von Rißflankeneffekten auf das Rißwiderstandsverhalten von Al_2O_3- Keramik*, [in:] Mikrobruchvorgänge in Al_2O_3-Keramik. DFG-Kolloquium, H. NICKEL and R.W. STEINBRECH [Eds.], pp. 57–89, Forschungszentrum Jülich 1991.
6. D. MUNZ and T. FETT, *Mechanisches Verhalten keramischer Werkstoffe*, Springer-Verlag, Berlin 1989.
7. J. LEMAITRE, *A course in damage mechanics*, Springer-Verlag, Berlin 1992.
8. J. NAJAR, *Continuous damage of brittle solids*, [in:] Continuum Damage Mechanics. Theory and Applications, D. KRAJCINOVIC and J. LEMAITRE [Eds.], pp. 233–294, Springer, Wien - New York 1987.
9. J. NAJAR, *Brittle residual strain and continuum damage at variable uniaxial loading*, Int. J. Damage Mech., **3**, 2, 260–276, 1994.
10. V.V. SILBERSCHMIDT and J. NAJAR, *Computational modelling of the size effect of damage inhomogeneity in ceramics*, Comput. Materials Sci. [in print].
11. J.B. WATCHMAN, *Mechanical properties of ceramics*, John Wiley & Sons, New York 1996.
12. A.L. GURSON, *Continuum theory of ductile rupture by void nucleation and growth. Part I. Yield criteria and flow rules for porous ductile media*, J. Engng. Mater. Technol., **99**, 1, 2–15, 1977.
13. O. BEER, *Verdichtung von Metallpulvern*, VDI Verlag, Düsseldorf, **5**, 458, 1996.
14. S. SHIMA and K. MIMURA, *Densification behaviour of ceramic powder*, Int. J. Mech. Sci., **28**, 1, 53–59, 1986.
15. H.J. HERRMANN and S. ROUX [Eds.], *Statistical models for the fracture of disordered media*, North Holland, Amsterdam 1990.
16. A. DELAPLACE, G. PIJAUDIER-CABOT and S. ROUX, *Progressive damage in discrete models and consequences on continuum modelling*, J. Mech. Phys. Solids, **44**, 1, 99–136, 1996.

17. V.V. SILBERSCHMIDT, *Mathematical modelling and fractal analysis of stochastic fracture process*, [in:] Mathematical Modelling and Applied Mathematics. Proc. IMACS Conf., A.A. SAMARSKY and M.P. SAPAGOVAS [Eds.], pp. 399–406, Elsevier Science Publishers B.V., North Holland, 1992.

18. V.V. SILBERSCHMIDT and J.-L. CHABOCHE, *The effect of material stochasticity on crack-damage interaction and crack propagation*, Engng. Fracture Mech., **48**, 3, 379–387, 1994.

19. C.W. MARSCHALL and A. RUDNICK, *Conventional strength testing of ceramics*, [in:] Fracture Mechanics of Ceramics. Volume 1. Concepts, Flaws and Fractography, R.C. BRANDT, D.P.H. HASSELMAN and F.F. LANGE [Eds.], pp. 69–92, Plenum Press, New York - London 1973.

LEHRSTUHL A FÜR MECHANIK
TECHNISCHE UNIVERSITÄT MÜNCHEN
Boltzmannstr. 15, D-85748 Garching b. München, Germany
e-mail: najar@lam.mw.tu-muenchen.de

Received July 18, 1997.